Supplementary information:
Recurrence-based reconstruction of dynamic pricing attractors

Shuixiu Lu and Sebastian Oberst

Recurrence-based reconstruction is applied in deterministic and stochastic systems to show the features of low-dimensional attractors and stochastic dynamics. We take six systems as benchmarking systems to support demand dynamics. The Rössler and the Duffing systems represent deterministic dynamics. Non-auto Fitzhugh-Nagumo model and a stochastic resonance in Duffing oscillator represent deterministic dynamics contaminated by different levels of noise. An AR(2) process and multi-fractional Gaussian noise represent stochastic dynamics.

1 Benchmark systems

The demand process [13] that we study has on-peak and off-peak patterns (Fig. 4C), we therefore utilize the systems that has different patterns in the time series. Table S1 gives the parameters and the equations of individual systems and indicates the corresponding dynamics.

Table S1: Deterministic and stochastic systems as the benchmarking dynamics. Eq. (S1) describes the Rössler system [14] by the $x-$, the $y-$, and the $z-$ components in the form of a first order differential equation. Eq. (S2) describes the Duffing oscillator [11] in the form of a second order differential equation. Eq. (S3) describes a stochastic resonance (SR) [2, 6] by optimizing the noise level that a periodic Duffing oscillator involves. Eq. (S4) describes the non-auto FitzHugh-Nagumo model (nFHN) [5] by the $v-$ and the $w-$ components in the form of a first order differential equation. The multi-fractional Gaussian noise (mfG) is obtained by a Python package [4]. The study in Ref. [3] is followed, and the Hurst exponent of the mfG depends on time, thus sinusoidally increasing from 0.25 to 0.75. The SR and the nFHN have different signal-to-noise ratio (SNR). Eq. (S5) describes an autoregressive (AR) model of order 2 by involving time delays.

System	Equations		Parameters	Dynamics
Rössler	$\begin{cases} \dot{x} = -y - z \\ \dot{y} = x + ay \\ \dot{z} = b + z(x - c) \end{cases}$	(S1)	$a = 0.1, b = 0.2, c = 3$	Periodic
			$a = 0.1, b = 0.2, c = 14$	Chaotic
Duffing	$\ddot{x} + \delta\dot{x} + \alpha x + \beta x^3 = Acos(\omega t)$	(S2)	$\delta = 0.3, \alpha = -1, \beta = 1, A = 0.37, \omega = 1.2$	Periodic
			$\delta = 0.05, \alpha = -1, \beta = 1, A = 0.33, \omega = 1.3$	Chaotic
SR	$\ddot{x} + \delta\dot{x} + \alpha x + \beta x^3 = Asin(\omega t) + D\xi(t)$	(S3)	$\delta = 0.5, \alpha = -1, \beta = 0.5, \omega = 0.09,$ $A = 0.38, D = 1, \xi(t)$: Gaussian noise $SNR = 26.85$ dB	Stochastically driven
nFHN	$\begin{cases} \dot{v} = v - v^3 - w + I_{\text{ext}}(t) \\ \tau\dot{w} = v - a - bw \end{cases}$	(S4)	$a = -0.3, b = 1.4, \tau = 20$ $I_{\text{ext}} \sim \mathcal{N}(0, 0.5)$: Gaussian noise $SNR = 8.14$ dB	Stochastically driven
mfG	-			Stochastic
AR(2)	$x_t = a + bx_{t-1} + cx_{t-2} + \epsilon_t$	(S5)	$a = 1, b = -1, c = 0.5, \epsilon_t$: Noise	Stochastic

The Rössler system (Rössler) [14] is quantified by $x-$, $y-$, and $z-$components (Table S1). The system can exhibit periodic and chaotic dynamics, depending on the value of the parameters. The system has suddenly bursting behaviors in $z-$component [7]. Generally, the dynamics is studied on $x-$ or $y-$component, or the three components together [3,12]. However, our focus is on a univariate time series with different patterns in dynamics. The experiment is thus conducted on $z-$component.

The forced damped double-well Duffing oscillator (Duffing) [11] can also exhibit periodic and chaotic dynamics. The system has been used to model the damped and forced vibrations in many engineered systems [7,11]. Under the parameters we choose, the system oscillates between two symmetric potential wells and exhibits a cross-well behavior. The oscillation presents different time scales in dynamics [11]. The slow dynamics is associated with the decaying of oscillations in a slow time scale [11]. The fast dynamics is associated with the damped natural frequency in a fast time scale [11].

Non-auto FitzHugh-Nagumo model (nFHN) [5] and stochastic resonance (SR) [2,6] have deterministic components, however, the driven force is Gaussian noise (Table S1). Stochastic resonance is a phenomenon taking place when a nonlinear signal is amplified and optimized by the presence of noise [2,6]. The system has been applied to model climate changes [1]. For a given strength of a periodic force, an optimal intensity of noise exists [2,6], resulting in an SR. An nFHN model exhibits the slow and the fast dynamics [10] and can describe an excitable system, such as the brain dynamics [16]. An SR and an nFHN models are with stochastically driven dynamics and represent deterministic systems contaminated by different levels of noise. Signal-to-noise ratio (SNR) measures the degree of deterministic dynamics in a system. The higher the SNR is, the higher level of determinism a system contains.

The multi-fractional Gaussian noise (mfG) and an AR(2) process have stochastic dynamics. Following the study in [3], we use the mfG and the AR(2) to show the feature of stochastic dynamics in recurrence plots. In addition, the mfG and the SR have a periodic modulation, cf. Table S1. We benchmark the mfG against the SR to show the features between stochastic systems and deterministic systems contaminated by an optimal level of noise.

In Eq. (S1) the parameters a and b are fixed, however, the parameter c determines the dynamics of the system. Eqs. (S2) and (S3) model damped and driven oscillators in engineered systems and have some common parameters. Here, x stands for the displacement at time t, $\dot{x}$ is the first order derive of x with respect to t and stands for the velocity, and $\ddot{x}$ is the second order derive of x with respect to t and stands for the acceleration, δ is the damping parameter, α and β are the linear and the nonlinear stiffness parameters, respectively. Either $Acos(\mathrm{A}t)$ (Eq. S2) or $Asin(\omega t)$ (Eq.S3) is the driving force of the Duffing oscillator where A controls the amplitude (strength) of the forcing and ω controls the frequency of the forcing. A difference between Eqs. (2) and (3) is a consideration of noise. In Eq. (S3), D stands for the intensity of noise. For a given A, an optimal D exists in detecting the underlying nonlinear oscillations [2,6]. This leads to an SR (Eq. S3). Eq. (S4) describes an excitable system to model brain dynamics [5,8]. Here, v and w stands for the membrane potential and the recovery variable, respectively [8], a and b are the coefficients, τ is a time scale parameter that control the slow dynamics (the recovery), and I_{ext} is an external stimulus that depends on time [8].

2 Pareto front and reordered front

A difference exists between the Pareto and the reordered fronts. For Pareto optimal solutions to Eq. (5), an increase of $\mathrm{SD_{DET}}$ implies a decrease of $\mathrm{SD_{TT}}$. In the (m, $\mathrm{SD_{TT}}$)-plane, however, the connection between m and $\mathrm{SD_{TT}}$ does not exist. We therefore increase m and keep the corresponding $\mathrm{SD_{TT}}$. If more than two Pareto optimal solutions exist at some m, then the largest $\mathrm{SD_{TT}}$ is chosen as the point to outline the reordered front. This suggests at a given m the Pareto optimal solutions without the largest $\mathrm{SD_{TT}}$ is regarded as the dominated solutions for a plot of the reordered front.

3 Algorithm to de-trend a time series

Algorithm: De-trend a time series by a linear regression

Result: Detrended demand

Input: A time series of raw demand $\{y_1, , y_2, \cdots, y_{N_p}\}$, where N_p is the total length;

for $t \in \{11, 12, y_{N_p} - 11\}$ **do**

  Make a linear regression of the data $\{(0, y_{t-10}), (1, y_{t-9}), \cdots, (10, y_t), \cdots, (20, y_{t+10})\}$;

  Fit the linear regression and calculate the prediction at the point $(10, y_t)$, which results in a linear fit $(10, \hat{y}_t)$;

  Return $y_t - \hat{y}_t$;

end

Yield a time series $\{y_t - \hat{y}_t\}_{t=11}^{N_p-11}$ of detrended demand;

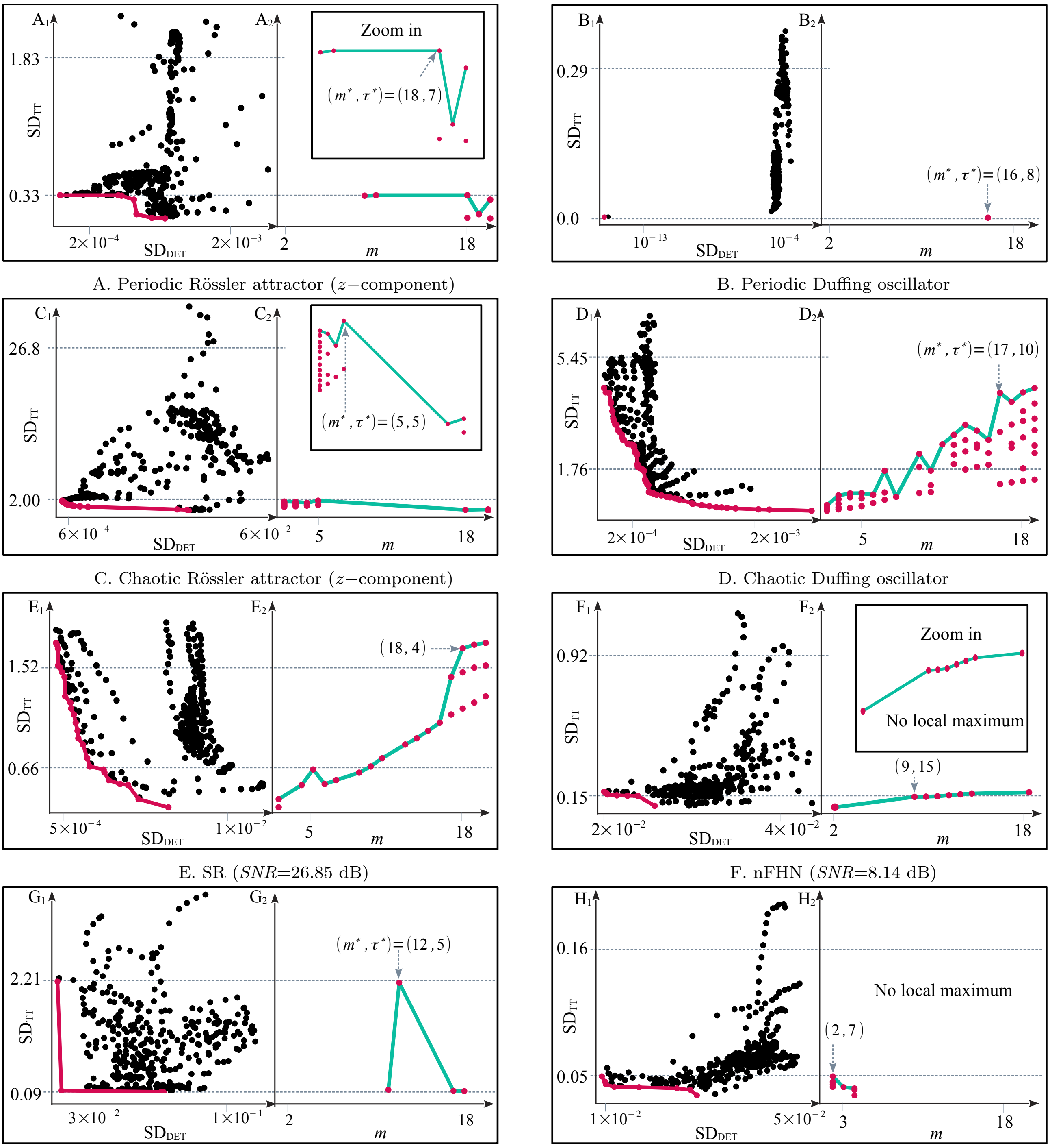

A. Periodic Rössler attractor (z−component)

B. Periodic Duffing oscillator

C. Chaotic Rössler attractor (z−component)

D. Chaotic Duffing oscillator

E. SR (SNR=26.85 dB)

F. nFHN (SNR=8.14 dB)

G. mfG

H. AR(2) process

Fig. S1. Pareto front and reordered front for benchmarking systems. A_1 to H_1: Pareto front is outlined by the corresponding Pareto optima of Eq. (5) in the $(\mathrm{SD_{DET}}, \mathrm{SD_{TT}})$-plane. Here, the x−axis is in a logarithmic scale. A_2 to H_2: The corresponding Pareto front of A_1 to H_1 is reordered in the $(m, \mathrm{SD_{TT}})$-plane. A and B: For periodic dynamics, the maximum of local maxima coincides with the global maximum in the reordered front. C and D: For chaotic dynamics, the feature of reordered front is similar to periodic dynamics. E and F: For stochastically driven dynamics where noise drives the system, the feature depends on the signal-to-noise ratio (SNR). G to H: For stochastic dynamics, the mfG exhibits the feature that a local maximum coincides with the global maximum in the reordered front. Nevertheless, the AR(2) process has no local maximum.

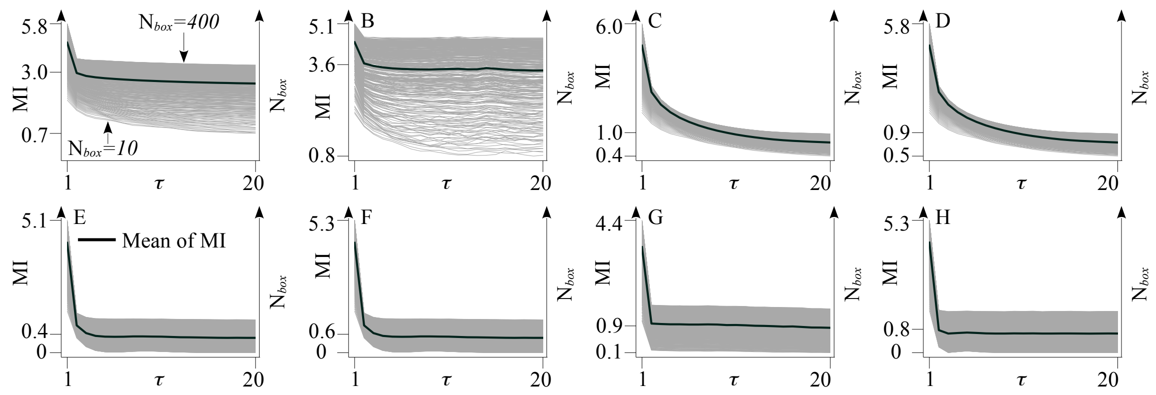

Fig. S2. Evident oscillations in averaged mutual information (MI) do not exist in locating the time delay dimension τ. A. Periodic Rössler attractor. B. Periodic Duffing oscillator. C. Chaotic Rössler attractor. D. Chaotic Duffing oscillator. E. SR. F. nFHN. G. mfG. H. An AR(2) process. Here, MI is calculated by calling the TISEAN package [9], where the number of boxes (N_{box}) increases from 10 to 400. The mean of MI is the mean of MI over all boxes.

Table S2: Features of the Pareto front in benchmarking systems with respect to the $x-$axis and the $y-$axis of Fig. S1A$_1$ to H$_1$. For periodic and chaotic dynamics, $SD_{\rm DET}$ covers at least two logarithmic scales, evidenced by maximum/minimum > 10. For stochastic driven dynamics, the feature of $SD_{\rm DET}$ depends on *SNR*. The SR with *SNR*=26.85 dB covers two logarithmic scales. However, the nFHN with *SNR*=8.14 dB is unable to cover two logarithmic scales, evidenced by maximum/minimum < 10 ($SD_{\rm DET}$). For stochastic dynamics, neither mfG nor AR(2) has $SD_{\rm DET}$ that covers two logarithmic scales. For SR and AR(2), their $y-$axis fluctuates in one logarithmic scale, evidenced by maximum/minimum < 10 ($SD_{\rm TT}$).

System	$SD_{\rm DET}$ ($x-$axis)			$SD_{\rm TT}$ ($y-$axis)		
	minimum	maximum	$\frac{\text{maximum}}{\text{minimum}}$	minimum	maximum	$\frac{\text{maximum}}{\text{minimum}}$
Periodic Rössler	1.2×10^{-4}	3.6×10^{-3}	30	7.3×10^{-2}	2.29	31.37
Periodic Duffing	2.2×10^{-16}	8.5×10^{-4}	3.9×10^{12}	3.6×10^{-15}	3.6×10^{-1}	10^{14}
Chaotic Rössler	5.3×10^{-4}	7×10^{-2}	132.08	3.8×10^{-1}	3.4×10^{1}	89.47
Chaotic Duffing	1.1×10^{-4}	6×10^{-3}	54.55	4.5×10^{-1}	6.82	15.16
SR	4.4×10^{-4}	1.9×10^{-2}	43.18	3.4×10^{-1}	1.9	5.59
nFHN	2×10^{-2}	4.5×10^{-2}	2.25	9.4×10^{-2}	1.14	12.13
mfG	2.4×10^{-2}	1.3×10^{-1}	5.42	9×10^{-2}	3.87	43
AR(2)	9.6×10^{-3}	5.5×10^{-2}	5.73	3.4×10^{-2}	2×10^{-1}	5.88

4 Results in benchmarking systems

The six benchmarking systems (Table S1) are applied with recurrence-based attractor reconstruction (Fig. 1 and Eq. 5). We will show the features of benchmarking systems from four aspects. They are the Pareto and the reordered fronts, recurrence plots under (m^*, τ^*), a statistics of DET and that of TT, and reconstructed attractors. Finally, we will benchmark the dynamics of ride-sharing demand and provide a decision matrix to summarize the results.

4.1 Pareto and reordered fronts

Fig. S1 shows Pareto optimal solutions to Eq. (5) in the benchmarking systems and outlines the Pareto and the reordered fronts. Three observations are obvious to distinguish between deterministic, stochastic, and stochastically driven dynamics, which are (i) the number of logarithmic scales in $SD_{\rm DET}$, (ii) a plateau shown in the Pareto front, and (iii) a local maximum in the reordered front.

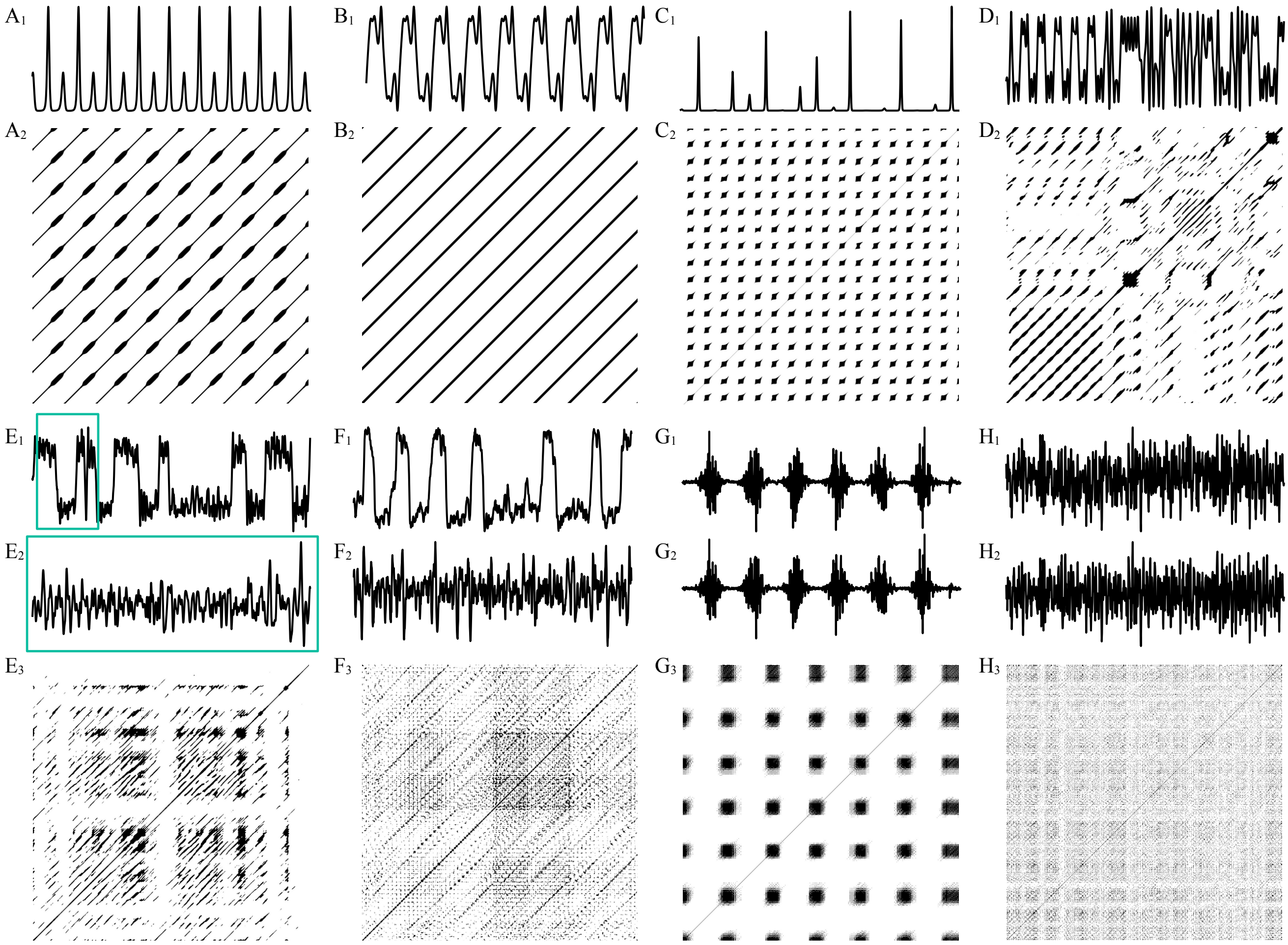

Fig. S3. Time series and recurrence plots of benchmarking systems. A_1 to D_1 are the time series. A_2 to D_2 are corresponding recurrence plots. E_1 to H_1 are an original time series. E_2 to H_2 are corresponding detrended time series. E_3 to H_3 are a recurrence plot of corresponding detrended time series. A. Dynamics of periodic Rössler attractor is shown at $(m^*, \tau^*) = (18, 7)$. B. Dynamics of periodic Duffing oscillator is shown at $(m^*, \tau^*) = (16, 8)$. C. Dynamics of the chaotic Rössler attractor is shown at $(m^*, \tau^*) = (5, 5)$. D. Dynamics of chaotic Duffing oscillator is shown at $(m^*, \tau^*) = (17, 10)$. E. Dynamics of the SR is shown at $(m^*, \tau^*) = (18, 4)$. F. Dynamics of the nFHN is shown at $(m^*, \tau^*) = (9, 15)$. G. Dynamics of the mfG is shown at $(m^*, \tau^*) = (12, 5)$. H. Dynamics of the AR(2) process is shown at $(m^*, \tau^*) = (2, 7)$. Fig. S1 provides the calculation of the corresponding (m^*, τ^*).

The number of logarithmic scales in $\mathrm{SD_{DET}}$. For deterministic dynamics, $\mathrm{SD_{DET}}$ varies at least in two different logarithmic scales (Fig. S1A_1 to D_1). For stochastically driven dynamics, the number of logarithmic scales depends on the *SNR*. The *SNR* in SR is 26.85 dB. The $\mathrm{SD_{DET}}$ covers from 10^{-4} to 10^{-2} (Fig. S1E_1) with maximum/minimum = 43.18 (Table S2). Here, the "maximum" ("minimum") is the maximum (minimum) of $\mathrm{SD_{DET}}$ over all choices of (m, τ). The *SNR* of nFNH is 8.14 dB, and the maximum/minimum = 2.25 < 10 (Table S2). This indicates that only one logarithmic scale is enough to cover $\mathrm{SD_{DET}}$ for all choices of (m, τ).

For stochastic dynamics, the ratio of the maximum of $\mathrm{SD_{DET}}$ and the minimum of $\mathrm{SD_{DET}}$ is less than 10 (Fig. S1G_1 and H_1 and Table S2). This indicates that it is difficult to reduce $\mathrm{SD_{DET}}$ by a factor of 10 using different choices of (m, τ) in recurrence plots. The $x-$axis in Fig. S1G_1 has two different logarithmic scales, 10^{-3} and 10^{-2}. However, the maximum/minimum = 5.42 (Table S2). This indicates that rescaling $\mathrm{SD_{DET}}$ allows only one logarithmic scale to cover all the variations in the $x-$axis of Fig. S1G_1.

A plateau shown in the Pareto front. For deterministic dynamics, its Pareto front shows one of the two phenomena. (1) A unique solution (m^*, τ^*) to Eq. (5) exists. At (m^*, τ^*) $\mathrm{SD_{DET}}$ and $\mathrm{SD_{TT}}$ simultaneously reach the minimum. For example, periodic Duffing oscillator has a unique solution at $(m^*, \tau^*) = (16, 8)$, cf. Fig. S1B$_1$. (2) An obvious plateau exists in the Pareto front. A plateau is a flat area satisfying the following two properties. (i) $\mathrm{SD_{DET}}$ covers at least two logarithmic scales ($x-$axis); and, (ii) the points that sit around the plateau have a relative small variation in the $y-$axis. For example, Fig. S1A$_1$ presents a plateau at the beginning part in the Pareto front, as evidenced by two observations. (1) $\mathrm{SD_{DET}}$ covers two logarithmic scales, 10^{-4} and 10^{-3}, cf. Fig. S1A$_1$, with maximum/minimum = 30 (Table S2), and (2) the $y-$axis of the plateau is around 0.33 (Fig. S1A$_1$). Similarly, a plateau can be seen in Fig. S1C$_1$ and D$_1$. For stochastically driven dynamics and stochastic dynamics, no obvious plateau exists. The $y-$axis of Fig. S1E$_1$ changes drastically, causing a lack of an area with a small variation in $\mathrm{SD_{TT}}$. In Fig. S1F$_1$ to G$_1$, the $x-$axis does not cover two different logarithmic scales, shown by maximum/minimum < 10 in $\mathrm{SD_{DET}}$ (Table S2).

Reordered front. We then look at the feature of the reordered front. For deterministic dynamics, it exists either at least one local maximum (Fig. S1A$_2$, C$_2$, and D$_2$) or a unique optimal solution (Fig. S1B$_2$). For stochastically driven dynamics and stochastic dynamics, it exists at most one local maximum (Fig. S1E$_2$ to H$_2$). In addition, for stochastic dynamics the Pareto optimal embedding dimension (m) clusters around some value (Fig. S1G$_2$ and H$_2$). Fig. S1G$_2$ presents that the mfG has no Pareto optimal m that is less than 11. The AR(2) process has no Pareto optimal m strictly larger than 5, cf. Fig. S1H$_2$.

Furthermore, in the reordered front a coincidence between the maximum of local maxima and the global maximum indicates different types of dynamics. For deterministic dynamics, the maximum of local maxima is either a global maximum (Fig. S1A$_2$ to C$_2$) or close to it (Fig. S1D$_2$). For stochastically driven dynamics, a local maximum either does not exist (Fig. S1F$_2$) or is distant from (Fig. S1E$_2$) the global maximum. For stochastic dynamics, the coincidence is observed in mfG (Fig. S1G$_2$). However, the Pareto front of the mfG is completely different with deterministic dynamics (Fig. S1A$_1$ to D$_1$ and G$_1$). For example, no plateau can be observed in the Pareto front of the mfG (Fig. S1G$_1$).

Locate the time delay τ for recurrence analysis Fig. S2 shows that the standard approach based on mutual information and false nearest neighbors is difficult to locate τ for the time series we study . The periodic (Fig. S2B) and the chaotic (Fig. S2D) Duffing oscillators have the first local minimum at $\tau = 9$ and $\tau = 12$, respectively. Also, SR (Fig. S2E), nFHN (Fig. S2F), and AR(2) (Fig. S2H) have the first local minimum at $\tau = 15$, $\tau = 6$, and $\tau = 8$, respectively. However, obvious oscillations, which are shown by multiple local maxima and minima [15], cannot be observed as mutual information is plotted against an increase of τ (Fig. S2). The claim that τ at the first local minimum is suitable for recurrence plots is inconclusive. In this situation, Pareto and reordered fronts provide an alternative way to find m and τ for recurrence analysis and attractor reconstructions.

4.2 Recurrence plots

Fig. S3 shows recurrence plots of benchmarking systems at (m^*, τ^*) derived from the corresponding reordered front (Fig. S1A$_2$ to H$_2$). For periodic dynamics shown in Fig. S3A$_2$ and B$_2$, recurrence plots exhibit non-interrupted diagonal lines. The distance between diagonal lines is related to the periodicity of a signal [12]. For the chaotic Rössler attractor, recurrence plot exhibits a switch between clusters of points and blank white areas (Fig. S3C$_2$), indicating a heterogeneity in dynamics. For the chaotic Duffing oscillator, recurrence plot contains long diagonal lines (Fig. S3D$_2$). However, those lines are interrupted by different patterns. For example, in Fig. S3D$_2$, there is a patch of non-interrupted diagonal lines similar to that of Fig. S3A$_2$. The different patterns correspond to the cross-well behavior of the chaotic Duffing oscillator [11].

For stochastically driven dynamics, long diagonal lines in SR indicate that determinisms exist (Fig. S3E$_3$). However, an increase of noise level can destroy the diagonal lines (Fig. S3F$_3$). For stochastic dynamics, the AR(2) process presents many isolated black points in Fig. S3H$_3$, whereas the mfG exhibits a switch between clusters and blank white areas in Fig. S3G$_3$. Fig. S3E$_1$ shows the cross-well behavior of an SR, which is consistent with the study of an SR in Ref. [3]. It is worth mentioning that Fig. S3E$_2$ corresponds to a segment of the detrended time series. Fig. S3E$_3$ is the recurrence plot of that segment, which is different from the plot shown in Ref. [3].

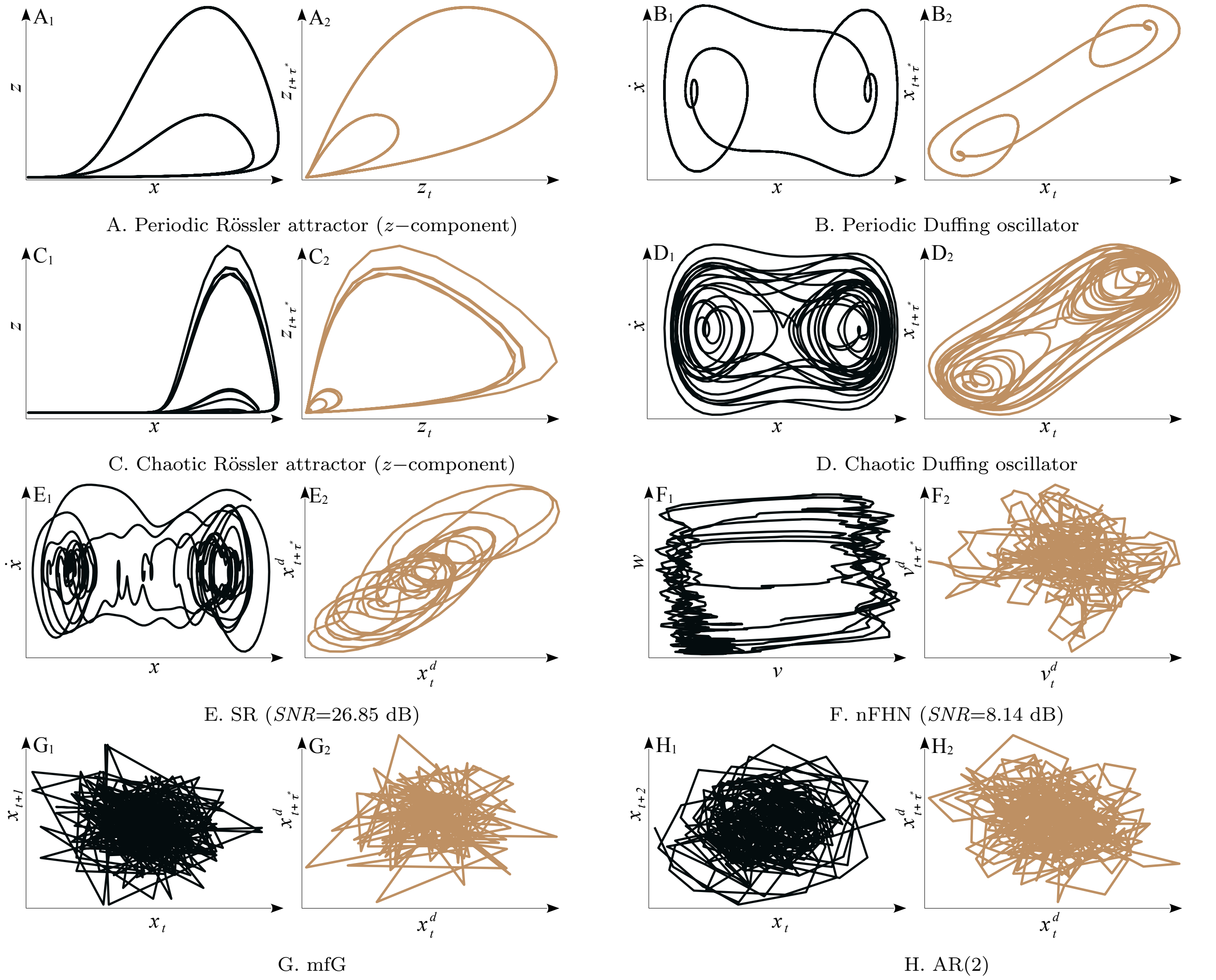

Fig. S4. Original and reconstructed attractors in benchmarking systems. A_1 to H_1: An original attractor. A_2 to H_2: Reconstructed attractor. A_2 to D_2: Attractors are reconstructed from the corresponding original time series shown in Fig. S3A_1 to D_1, respectively. E_2 to H_2: Attractors are reconstructed from the corresponding detrended time series (^{d}) shown in Fig. S3E_2 to H_2, respectively.

4.3 Reconstructed attractor at (m^*, τ^*)

Fig. S4 shows a phase plot of an original attractor and that of the reconstructed attractor at (m^*, τ^*). For deterministic dynamics (Fig. S4A to D), the reconstructed attractors preserve the topological structures of corresponding original attractors. For example, the Duffing oscillator (Fig. S4B_1 and D_1) exhibits double occurrences of the scroll-and-squeeze phenomenon [7]. The reconstructed attractors (Fig. S4B_2 and D_2) preserver that phenomenon. For stochastic driven dynamics, the SR is with high determinism, the reconstructed attractor shows deterministic structures (Fig. S4E_2). However, the double wells of SR are destroyed (Fig. S4E). The reconstructed attractor of nFHN is incapable of preserving the structure of the original attractor in phase plot (Fig. S4F). For stochastic dynamics, the reconstruction does neither preserve nor distort the original phase plot (Fig. S4G and H).

4.4 Patterns of DET and TT

Fig. S5 shows how μ_{DET} and μ_{TT} change as $l_{\min}$ and $v_{\min}$ change, respectively. While μ_{DET} monotonically decreases as $l_{\min}$ increases (Fig. S5A_1 to A_4), μ_{TT} firstly increases and then decreases as $v_{\min}$ increases (Fig. S5B_1 to B_4).

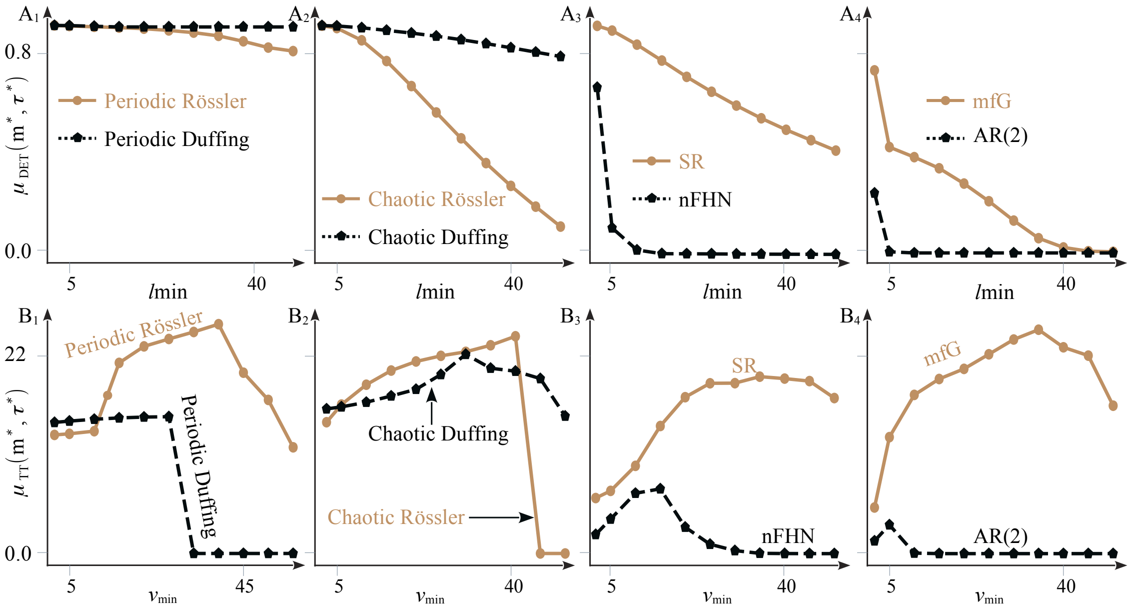

Fig. S5. Patterns of DET (Eq. 3) and TT (Eq. 4) as $l_{\min}$ and $v_{\min}$ increase. A_1 to A_4 are the patterns of μ_{DET} as $l_{\min}$ is varied. B_1 to B_4 are the patterns of μ_{TT} as $v_{\min}$ is varied. Here, μ_{DET} and μ_{TT} are calculated via Eq. (5). A_1 and B_1: Periodic Rössler attractor and periodic Duffing oscillator. A_2 and B_2: Chaotic Rössler attractor and chaotic Duffing oscillator. A_3 and B_3: The SR and the nFHN. A_4 and B_4: The mfG and the AR(2) process.

The phenomenon is due to a different definition of DET and TT. The value of $l_{\min}$ only affects the numerator of DET (Eq. 3). However, the value of $v_{\min}$ affects both the numerator and the denominator of TT (Eq. 4).

For periodic dynamics, the change of $l_{\min}$ has a relative small influence on μ_{DET}. The periodic Rössler attractor and the periodic Duffing oscillator show a μ_{DET} larger than 0.8 at $l_{\min} = 50$ (Fig. S5A_1). For chaotic dynamics, μ_{DET} presents two features. (i) At $l_{\min} = 50$, μ_{DET} does not go to zero (Fig. S5A_2). However, (ii) the slope of the curve depends on individual systems. Fig. S5A_2 shows that the chaotic Rössler attractor decreases faster than the chaotic Duffing oscillator.

For stochastically driven dynamics, the feature of μ_{DET} depends on the *SNR*. The SR contains a high level of determinisms where *SNR*=26.85 dB and shows a similar pattern as the chaotic Rössler attractor and the chaotic Duffing oscillator (Fig. S5A_2 and A_3). Nevertheless, for the nFHN where *SNR*=8.14 dB, its μ_{DET} goes to zero at $l_{\min} = 10$. For stochastic dynamics, $\mu_{\mathrm{DET}} = 0$ for both the mfG and the AR(2) process at $l_{\min} = 50$ (Fig. S5A_4). The AR(2) process shows a quicker way to approach zero than the mfG. Furthermore, as $l_{\min}$ increases from 2 to 5, μ_{DET} abruptly decreases related to the nFHN, the mfG, and the AR(2) process (Fig. S5A_3 and A_4).

Fig. S5B shows the pattern of μ_{TT} as $v_{\min}$ increases. For periodic dynamics, μ_{TT} has a plateau at the beginning (Fig. S5B_1). For the chaotic Rössoler attractor and the chaotic Duffing oscillator (Fig. S5B_2), μ_{TT} increases firstly and then abruptly decreases as $v_{\min}$ increases. The amplitude of the increase is relatively small. For stochastically driven dynamics, a common feature is that a plateau exists in the middle (Fig. S5B_3), despite a short length for the nFHN. For stochastic dynamics, both the mfG and the AR(2) process present a downward "V" (Fig. S5B_4).

5 Decision matrix

We compare the feature of ride-sharing demand with the benchmarking systems and provide a decision matrix to score the results, cf. Table S3. A score, ranging from 0 to 1, indicates the confidence in concluding ride-sharing demand dynamics.

For example, when scoring the feature, the number of logarithmic scales in $\mathrm{SD}_{\mathrm{DET}}$ (Table S3), we compare the patterns between the ride-sharing demand and the benchmarking systems. The comparison is based on the $x-$axis of Fig. 4A_1 and that of Fig. S1A_1 to H_1. The maximum of and the minimum of $\mathrm{SD}_{\mathrm{DET}}$ in the ride-sharing demand

Table S3: Decision matrix to summarize the features of ride-sharing demand for dynamics identifications. Here, “S” indicates a score of 0 as the feature follows the pattern of stochastic dynamics, and “D” indicates a score of 1 as the feature follows the pattern of deterministic dynamics. The feature in the Pareto and the reordered fronts is scored by comparing between Figs. S1 and 4. The feature of recurrence plots is scored by comparing between Figs. S3 and 4. The feature of DET and TT is scored by comparing between Figs. S5 and 6. The feature of reconstructed attractors is scored by Fig. 7.

Features	Pareto front			Recurrence	Patterns		Phase plot	Dynamics
	Logarithmic scales	Plateau	Maxima	plots	DET	TT	(Attractor)	
Ride-sharing demand	S	S	D	D	D	D	D	D
Poisson	S	S	S	S	S	S	S	S

are 0.051 and 0.012 (Fig. $4A_1$), respectively. The maximum/minimum is equal to 4.25 being less than 10. The feature is consistent with that of stochastic dynamics, as shown in Fig. $S1E_1$, G_1, H_1, and Table S2. In addition, a plateau is not observed in Fig. $4A_1$. We thus score “S” related to the two features, the number of logarithmic scales in SD_{DET} and a plateau in Pareto front (Table S3). However, the feature related to the local maxima in the (m, SD_{DET})-plane indicates a more likely conclusion of deterministic dynamics (Fig. $4A_2$). Two observations support the scoring of “D”. (i) Three local maxima are observed in the reordered front (Fig. $4A_2$), and m spans from 2 to 18 (Fig. $4A_2$). (ii) The maximum of local maxima coincides the global maximum in the reordered front (Fig. $4A_2$). Those features are consistent with deterministic dynamics (Fig. $S1A_1$ to D_1).

Fig. $4C_4$ further indicates a high confidence in concluding deterministic dynamics of the ride-sharing demand. The observations include (i) non-interrupted diagonal lines (Fig. $4C_4$), similar to the pattern in the periodic Rössler attractor (Fig. $S3A_2$) and in the periodic Duffing oscillator (Fig. $S3B_2$), and (ii) recurring long diagonal lines (Fig. $4C_4$), similar to that in the chaotic Duffing oscillator (Fig. $S3D_2$). The feature related to recurrence plots in Table S3 is thus scored with “D”.

References

1. Benzi, R., Parisi, G., Sutera, A., Vulpiani, A.: Stochastic resonance in climatic change. Tellus **34**(1), 10–16 (1982)
2. Benzi, R., Sutera, A., Vulpiani, A.: The mechanism of stochastic resonance. Journal of Physics A: mathematical and general **14**(11), L453 (1981)
3. Braun, T., Unni, V.R., Sujith, R., Kurths, J., Marwan, N.: Detection of dynamical regime transitions with lacunarity as a multiscale recurrence quantification measure. Nonlinear Dynamics pp. 1–19 (2021)
4. Christopher, F.: Python package for fractional brownian motion realizations. `https://pypi.org/project/fbm/` (2021). Accessed: 2021-05-09
5. FitzHugh, R.: Impulses and physiological states in theoretical models of nerve membrane. Biophysical journal **1**(6), 445–466 (1961)
6. Gammaitoni, L., Hänggi, P., Jung, P., Marchesoni, F.: Stochastic resonance. Reviews of modern physics **70**(1), 223 (1998)
7. Gilmore, R., Lefranc, M.: The Topology of Chaos. John Wiley & Sons, Inc (2011)
8. Guilhem, D.: Collected lecture notes in computation biology. `https://www.normalesup.org/~doulcier/teaching/modeling/excitable_systems.html` (2021). Accessed: 2021-05-09
9. Hegger, R., Kantz, H., Schreiber, T.: Practical implementation of nonlinear time series methods: The tisean package. Chaos: An Interdisciplinary Journal of Nonlinear Science **9**(2), 413–435 (1999)
10. Kasthuri, P., Pavithran, I., Krishnan, A., Pawar, S.A., Sujith, R., Gejji, R., Anderson, W., Marwan, N., Kurths, J.: Recurrence analysis of slow–fast systems. Chaos: An Interdisciplinary Journal of Nonlinear Science **30**(6), 063152 (2020)
11. Kovacic, I., Brennan, M.J.: The Duffing equation: nonlinear oscillators and their behaviour. John Wiley & Sons (2011)
12. Marwan, N., Romano, M.C., Thiel, M., Kurths, J.: Recurrence plots for the analysis of complex systems. Physics Reports **438**(5-6), 237–329 (2007)
13. RideAustin (2017): Ride-austin-june6-april13 [dataset] (2013). URL `https://data.world/ride-austin/ride-austin-june-6-april-13`. Accessed: 2021-05-19
14. Rössler, O.E.: An equation for continuous chaos. Physics Letters A **57**(5), 397–398 (1976)
15. Stender, M., Oberst, S., Tiedemann, M., Hoffmann, N.: Complex machine dynamics: systematic recurrence quantification analysis of disk brake vibration data. Nonlinear Dynamics **97**(4), 2483–2497 (2019)
16. Zhou, C., Zemanová, L., Zamora, G., Hilgetag, C.C., Kurths, J.: Hierarchical organization unveiled by functional connectivity in complex brain networks. Physical review letters **97**(23), 238103 (2006)